12th International Symposium on Turbulence and Shear Flow Phenomena (TSFP12)
Osaka, Japan (Online), July 19-22, 2022

ROUGHNESS EFFECTS MODELING WITH A DOUBLE AVERAGED NAVIER-STOKES TURBULENCE MODEL

François Chedevergne
DMPE, ONERA, Université de Toulouse
F-31055 Toulouse, France
francois.chedevergne@onera.fr

ABSTRACT

Recent progress of the discrete element method to account for roughness effects in wall bounded flows were obtained with the use of the double averaged Navier-Stokes equations (Chedevergne, 2021). A volume averaging technique was set up on the Reynolds averaged Navier-Stokes equations and a new model for the form drag was derived (Chedevergne & Forooghi, 2020). The whole model was tested on a large panel of DNS configurations but some complementary validation on high Reynolds configurations were still required. Besides, the central question regarding the inputs of the model from a randomly rough surface remained opened. The present paper aims at answering both issues by applying the developed model to a set of high Renyolds number boundary layer experimental configurations (Squire *et al.*, 2017) and by proposing a methodology of definition of the input parameters. The resulting process provides a representative elementary roughness from which very satisfactory agreements were obtained on the velocity profiles for all the tested Reynolds number.

INTRODUCTION #1

The modeling of turbulent boundary layers over rough surfaces is a long story which dates back to almost a century with the founding works of Nikuradse (1937) and Schlichting (1937). From these pioneer studies, the concept of equivalent sand grain, whose height is denoted k_s thereafter, was used in most of the modeling approaches. In particular, a large collection of corrections (Hellsten & Laine (1998); Knopp *et al.* (2009); Aupoix (2015)) dedicated to RANS turbulence models and relying on this concept were developed. However, several well-known drawbacks come along with all these corrections such as non-physical behaviors of turbulent quantities in the viscinity of the walls and the strong dependence to had-oc correlations to determine k_s values. Additionnally, specific modifications are required to asses heat transfer since the Reynolds analogy do not hold in the equivalent sand grain approach (Aupoix (2016)). Therefore, a more general approach was also developed to account for roughness effects in turbulent boundary layers.

The idea, introduced by Schlichting (1937), was to use blockage factors to mimic roughness effects. This led to the development of the discrete element method, especially thanks to studies by Finson (1982) Robertson (1961) Christoph & Pletcher (1983) Lin & Bywater (1982) or Taylor *et al.* (1985). Source terms are introduced in the mometum and energy equations to reproduce the viscous and form drags and heat transfer due to the roughness. The standard formulation of Taylor *et al.* (1985) rely on a simple drag model associated with a mixing length model. Although limited to boundary layer flows or channel (pipe) flows, this model was improved over the years and successfully applied in several configurations (McClain *et al.* (2006); Hosni *et al.* (1993)). More recently, the model was extended to RANS turbulence models (Stripf *et al.* (2008); Hanson *et al.* (2019)), the equations set still being derived from budgets on a control volume. Actually, Aupoix (2016) proved that the discrete element method can be derived through the use of a volume-averaging technique (Whitaker (1996)) leading to the Double Averaged Navier-Stokes (DANS) equations, initially devoted to fluids motion in porous media.

Until recently, the initial drag force model (Taylor *et al.* (1985)) was unquestioned. Yet, Chedevergne & Forooghi (2020) clearly pointed out the limit of the standard drag model and proposed an improved version. In parallel, Kuwata & Kawaguchi (2019) also found a drag model based on the Darcy-Forchheimer law, providing similar results, and demonstrating the need for a revisited discrete element model. The main difficulty is then to find a suitable turbulence model, compliant with the drag model and that reproduced observations made in the roughness sublayer. Kuwata *et al.* (2019) derived a DANS model based on a Reynolds stress model (Craft & Launder (1996)). It can be considered as the most advanced model of that type to deal with roughness issues in turbulent boundary layers. However, in their model, Kuwata *et al.* neglected the dispersive stresses, ensuing from the use of volume averaging, and do not consider heat transfer.

Recently, a complete DANS model dedicated to rough surfaces with heat transfer and relying on the $k-\omega$ SST model of Menter (1994) was proposed. The model was tested on a series of DNS databases and proved its ability to correctly reproduce the velocity profiles in the rouhness sublayer and the logarithmic region. To drive the model, the concept of representative elementary roughness (RER) was introduced to comply with the discrete element formalism. For academic roughness distributions, the definition of the RER is straightforward, but a process must be developed to extend the concept to randomly rough surfaces. Additionally, this DANS formulation was only validated on low-Reynolds configurations, quite far from most of the industrial applications. Therefore, this paper proposes a well-defined process to determine the RER and its application to a high-Reynolds boundary layer rough configuration Squire *et al.* (2017).

The DANS model

The model is detailed in Chedevergne (2021) and is briefly recap thereafter. First, the RANS equations are volume

averaged following Whitaker (1986). The blockage factor β, representing the volume fraction opened to the flow, is then introduced in the equations. For a viscous incompressible fluid, the resulting continuity and momentum equations read:

$$\begin{aligned}
&\frac{\partial \langle \beta \overline{u_i} \rangle^f}{\partial x_i} = 0 \\
&\frac{\partial \langle \overline{u_i} \rangle^f}{\partial t} + \langle \overline{u_j} \rangle^f \frac{\partial \langle \overline{u_i} \rangle^f}{\partial x_j} = -\frac{1}{\rho}\frac{\partial \langle \overline{p} \rangle^f}{\partial x_i} + \frac{1}{\beta}\frac{\partial}{\partial x_j}\left(\nu \frac{\partial \beta \langle \overline{u_i} \rangle^f}{\partial x_j}\right) \\
&\quad -\frac{1}{\beta}\frac{\partial}{\partial x_j}\left(\beta \left\langle \overline{u_i' u_j'} \right\rangle^f + \beta \overline{\tilde{u}_i \tilde{u}_j}\right) - \frac{\nu}{\beta}\frac{\partial \beta}{\partial x_j}\frac{\partial \langle \overline{u_i} \rangle^f}{\partial x_j} - \overline{F_{d_i}}
\end{aligned} \tag{1}$$

where the drag force F_{d_i} is defined by:

$$\begin{aligned}
F_{d_i} &= \frac{1}{S_f}\left(\int_{I_{fs}} \frac{\tilde{p}}{\rho} n_i ds - \int_{I_{fs}} \nu \frac{\partial \tilde{u}_i}{\partial x_k} n_k ds\right) \\
&= (1-\beta)\frac{2}{\pi d} C_d \| \langle \underline{u} \rangle^f \| \langle u_i \rangle^f = f_d \langle u_i \rangle^f
\end{aligned} \tag{2}$$

For years, the drag coefficient C_d was modeled following Taylor *et al.* (1985). Even though, some success were obtained with this simple model, in combination with the use of a standard turbulence model (McClain *et al.* (2004); Stripf *et al.* (2009); Hanson *et al.* (2019)), a comprehensive study of the drag force distribution based on DNS results showed the necessity of more complex modelings. Two models (Kuwata & Kawaguchi (2019); Chedevergne & Forooghi (2020)), having completely different roots, were found to adequately reproduce the drag forces obtained in the DNS. The present drag force (2) makes use of the formulation developed by Chedevergne & Forooghi (2020) which relies on the work of Žukauskas (1972) for banks of tubes in channel flows. Because of this link, only roughness having circular cross-sections can be considered. Then,

$$\beta = 1 - \frac{\pi d^2}{4 L_x L_z} \tag{3}$$

with d the roughness diameter and L_x and L_z the longitudinal and transverse spacings between roughness.
The drag coefficient is given by:

$$C_d = 1.5 (\alpha\beta)^2 \xi \tag{4}$$

where α is a parameter controlling the density and ξ is a decreasing function of the Reynolds number Re_d, based on the local roughness diameter d. More details can be found in Chedevergne & Forooghi (2020) and Chedevergne (2021).
The modeling of the Reynolds stress $-\left\langle \overline{u_i v_j} \right\rangle^f$ is made with a modified version of the $k-\omega$ SST model. Additional source terms are included in the turbulent scalar equations to force the desired behaviors in the roughness sublayer. The main idea is to aligned these sources terms with the drag force using function f_d (2). Thus, sources terms F_k and F_ω, respectively applied to k and ω equations, are given by:

$$\begin{aligned}
f_k &= c_k f_d \\
f_\omega &= \left(c_{\omega_1} + c_{\omega_2}\frac{1-\varphi}{\varphi}\right)\left(1 + c_{\omega_3}\exp\left(\frac{-1}{1-\beta_m}\right)\right) f_d
\end{aligned} \tag{5}$$

with $c_k = 2$, $c_{\omega_1} = 2.7$, $c_{\omega_1} = 0.1$ and $c_{\omega_1} = 30$. Geometrical parameters, φ, the effective element slope, and β_m, the mean blockage, were found to be the most influential on the turbulent properties within the roughness sublayer.
There exists no true model for the dispersive stresses $-\overline{\tilde{u}_i \tilde{u}_j}$ that can be used in the DANS equations (1). However, in the present context, the study is restricted to boundary layer configurations where only the $-\overline{\tilde{u}\tilde{v}}$ has to be provided. According to Chedevergne (2021) one writes:

$$\begin{aligned}
-\overline{\tilde{u}\tilde{v}} &= F_{disp}\nu_t \frac{\partial \sqrt{k}}{\partial y} \\
F_{disp} &= e^{-\left(\frac{y}{k_r} - 1\right)}
\end{aligned} \tag{6}$$

Representative Elementary Roughness

The boundary layer configurations examined in the present study are those of Squire *et al.* (2017) obtained in the large facility called High Reynolds Number Boundary Layer Wind Tunnel (HRNBLWT) at the University of Melbourne. For all these configurations, the wind tunnel floor was covered with a sandpaper for which an optical 3D scan was performed on a 25.4mm $\times$ 25.4mm sample. Surface statistics were extracted from this scan and it was shown (Squire *et al.*, 2017) that the distribution of roughness heights for the sandpaper surface is approximately normally distributed about the mean elevation $\overline{y}$. Figure 1 shows the scan of the sandpaper sample. To perform computations using the DANS model described above, a RER must be defined as explained by Chedevergne (2021). Actually, four parameters are necessary but this figure can be easily reduced to only two. First, considering only a RER with circular wall parallel cross-sections, *i.e.* for which relation (3) holds, limits the number of independent parameters. Second, by assuming an isotropic distribution of peaks and troughs on the surface, the spacings L_x et L_z can be reasonably taken as equals. Finally to define the RER, only the distributions of β and d are required, the spacing L_z being deduced from relation (3).

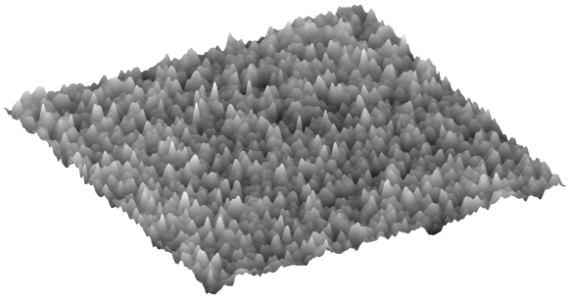

Figure 1. Scan of the sandpaper sample

The blockage factor β and the diameter d can be computed from the 3D scan for each altitude y using simple image processing. At a given altitude y, which origin $y = 0$ is taken as the bottom of the sandpaper sample, a planar slice is extracted and the image is binarized. Two examples are shown on figures 2a and 2a for $y = \overline{y} + 0.2$ mm and $y = \overline{y}$ respectively. The blockage factor $beta(y)$ is simply computed as the ratio of

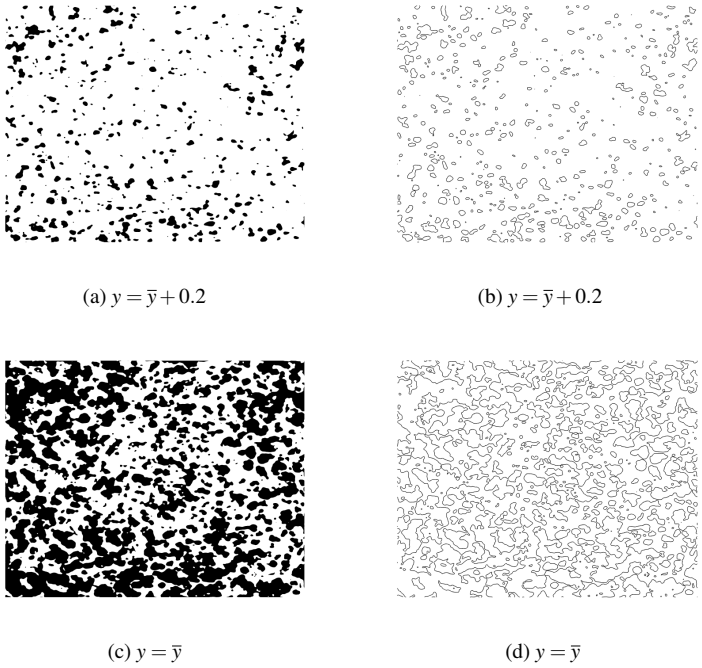

(a) $y = \overline{y} + 0.2$ (b) $y = \overline{y} + 0.2$

(c) $y = \overline{y}$ (d) $y = \overline{y}$

Figure 2. Images and contours of slices of the sandpaper sample of figure 1.

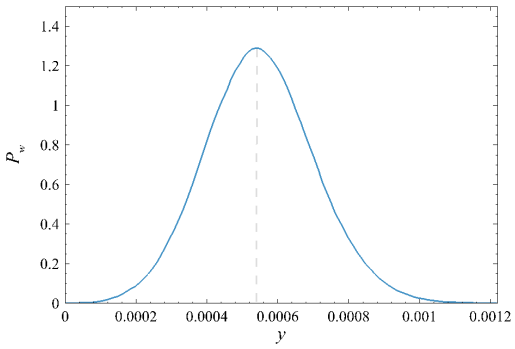

Figure 3. Wetted perimeter P_w as a function of the altitude y. The vertical dashed line shows the separation between k-type and d-type roughness behaviors located at $y = y_0$.

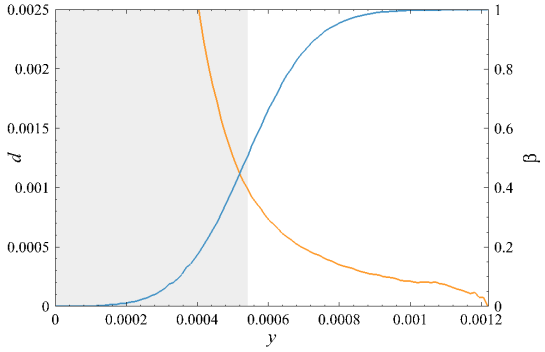

Figure 4. Blockage factor β (right) and diameter d with respect to the altitude y. The gray area represents the region below y_0 given in figure 3.

the area of the white region over the total surface, *i.e.* the ratio of the surface opened to the flow. To compute the diameter $d(y)$, we make use of the definition of the hydraulic diameter $d = \dfrac{4S_w}{P_w}$ with S_w the wetted surface and P_w wetted perimeter. Area S_w was already computed to access β. Perimeter P_w is computed as the sum of all the contour lengths in the image. Examples of image of contours are plotted on figures 2b and 2d. If for $y = \overline{y} + 0.2$ mm approximating the surface roughness distribution with circular cross-section appears to be quite obvious, this is far from being trivial at altitude $y = \overline{y}$. Final distributions of β and d with respect to y are given on figure 4, while the perimeter $P_w(y)$ is drawn on figure 3.

Before finalizing the process of building the RER, a recursive issue about the discrete element method for rough surface must be addressed. For randomly rough surfaces, some parts may not particpate to wall transfer. For instance, McClain *et al.* (2004) and McClain *et al.* (2006) pointed out the presence of dead water zones for dense rough configurations and defined the notion of "mean elevation" from the melt-down surface. This concept was also invoked by Aupoix (2016) to develop a thermal correction in the context of an equivalent sand grain model. More generally, the issue is related to the type of roughness encountered. Following Perry *et al.* (1969), a distinction is made between k-type and d-type roughness. The discrete element method, based on the introduction of a blockage factor, is strictly devoted to k-type roughness and is unable to predict the drag increase due to d-type roughness. More specifically, the drag models Taylor *et al.* (1985), citeKuwata19b or Chedevergne & Forooghi (2020) are all designed to reproduce the form drag of k-type roughness. For most of the surface of industrial interest, k-type and d-type roughness resemble the illustration of figure 5. For the present configuration, both types of roughness exist and must be distinguished. Starting from the

Figure 5. sketch of typical k-type roughness (left) and d-type roughness (right).

top of sandpaper surface, the wetted perimeter is growing as y is decreasing. This is a typical behavior encountered with k-type roughness. However, for y below $y_0 = 0.54$ mm, P_w is a monotonic increasing function of y, and roughness should be considered as d-type roughness. Practically, $beta$ and d are bounded by their lower values $\beta(y_0)$ and $d(y_0)$. The impact of this choice is very limited on the equations set (1) and the closure relation (4) since the flow is almost "blocked" in this region but this has a strong impact on the mean blockage value β_m that rules the source term in the ω-equation (5).

Results and discussion

Until now, the model was only tested at low Reynolds numbers from DNS configurations. The objective is to check the ability of the DANS model to reproduce boundary layers at high Reynolds values and to assess its sensitivity to variation of the Reynolds number. Among the experiments of Squire *et al.* (2017), 6 cases were retained for which dimensionless boundary layer thickness δ^+ ranges from less than 4000 to about 30000. Table 1 provides the main characteristics of these configurations.

To solve the DANS equations (1) we considered the inner region of boundary layer approximations. The convective terms were neglected and the equations were turned dimensionless using the kinematic viscosity ν and the friction velocity u_τ.

The origin of the y coordinate in the experimental data must be shifted since the reference was set to the roughness crest. We used the values obtained from the sample of figure 1 to rescale the coordinate inducing thus a slight uncertainty on the origin $y = 0$. This must not affect the experimental results, except in viscnity of the wall within the roughness sublayer. In addition, the wall correction parameter ε is taken as $\varepsilon = h/2$, with $h = 0.902$ mm the roughness height in compliance with the definitions given by Squire *et al.* (2017).

Profiles $u^+ = u/u_\tau$ are plotted on figure 6 for all configurations. An additional smooth profile is depicted on the figure. The corresponding computation was performed with the standard $k-\omega$ SST model Menter (1994).

As the Reynolds number δ^+ is increasing, the roughness function δu^+ increases too, shifting down the velocity profiles. The computed roughness functions are in very good agreement with the experimental ones with a relative error limited to 4%, except for the second configuration where it reached 12%. Some discrepancies occur when the profiles enter the roughness sublayers. It is hard to say whether it comes from the different models, the definition of the RER or some uncertainties in the measurements regarding the location of the probe. Nevertheless, the remarkable point of all these computations is that they were made from a single RER. The effect of the Reynolds number variations on this RER is very well captured by the whole DANS model. Besides, the methodology followed to define the RER on such a complex topology is efficient, even though reducing the rough surface to a unique roughness with a circular cross-section does not appear to be self-evident. Remark that it is hard to figure out the RER design because the spacings are not constant. There are indeed computed from the relation (3) and, in the present case, L_z ($= L_x$) is an increasing function of y for $y > y_0$.

Acknowledgment

The author is very grateful to D. Chung, N. Hutchins from Melbourne University and to M. MacDonald from the University of Auckland for sharing their data and knowledge on roughness issues. Model validation crucially depends on detailed experimental or numerical data and nothing would have been done without their support.

REFERENCES

Aupoix, B. 2015 Roughness Corrections for the $k-\omega$ Shear Stress Transport Model: Status and Proposals. *Journal of Fluids Engineering* **137**, 021202.

Aupoix, B. 2016 Revisiting the discrete element method for predictions of flows over rough surfaces. *Journal of Fluids Engineering* p. 31205.

Chedevergne, F. 2021 A double-averaged navier-stokes $k\omega$ turbulence model for wall flows over rough surfaces with heat transfer. *Journal of Turbulence* **0** (0), 1–22.

Chedevergne, F. & Forooghi, P. 2020 On the importance of the drag coefficient modelling in the double averaged navier-stokes equations for prediction of the roughness effects. *Journal of Turbulence* **21** (8), 463–482.

Christoph, G.H. & Pletcher, R.H. 1983 Predictions of rough-wall skin friction and heat transfer. *AIAA Journal* **21** (4), 509–515.

Craft, T.J. & Launder, B.E. 1996 A Reynolds stress closure designed for complex geometries. *International Journal of Heat and Fluid Flows* **17** (3), 245–254.

Finson, M.L. 1982 A model for rough wall turbulent heating and skin friction. AIAA Paper 82-0199 20^{th} Aerospace Science Meeting, Orlando, Florida.

Hanson, David R., Kinzel, Michael P. & McClain, Stephen T. 2019 Validation of the discrete element roughness method for predicting heat transfer on rough surfaces. *International Journal of Heat and Mass Transfer* **136**, 1217–1232.

Hellsten, A. & Laine, S. 1998 Extension of the $k-\omega$ shear-stress transport turbulence model for rough-wall flows. *AIAA Journal* **36** (9), 1728–1729.

Hosni, M.H., Coleman, H.W., Gardner, J.W. & Taylor, R.P. 1993 Roughness element shape effects on heat transfer and skin friction in rough-wall turbulent boundary layer. *International Journal of Heat and Mass Transfer* **36** (1), 147–153.

Knopp, T., Eisfeld, B. & Calvo, J.B. 2009 A new extension for $k-\omega$ turbulence models to account for wall roughness. *International Journal of Heat and Fluid Flow* **30**, 54–65.

Kuwata, Y. & Kawaguchi, Y. 2019 Direct numerical simulation of turbulence over resolved and modeled rough walls with irregularly distributed roughness. *International Journal of Heat and Fluid Flow* **77**, 1 – 18.

Kuwata, Y., Suga, K. & Kawaguchi, Y. 2019 An extension of the second moment closure model for turbulent flows over macro rough walls. *International Journal of Heat and Fluid Flow* **77**, 186–201.

Lin, T.C. & Bywater, R.J. 1982 Turbulence models for high-speed, rough-wall boundary layers. *AIAA Journal* **20** (3), 325–333.

McClain, S.T., Collins, S.P., Hodge, B.K. & Bons, J.P. 2006

Table 1. Details of the rough wall configurations.

U_∞	δ^+	u_τ	Δu^+ (exp.)	Δu^+ (DANS)	$\pm$ error (%)
4.7	3970	0.18	2.7	2.81	−4.1
10.1	9730	0.40	5.2	5.83	−12.1
15.2	14980	0.61	6.6	6.75	−2.3
20.6	20160	0.83	7.5	7.79	−3.9
25.4	25020	1.02	8.2	8.01	2.3
30.4	29900	1.23	8.6	8.58	0.2

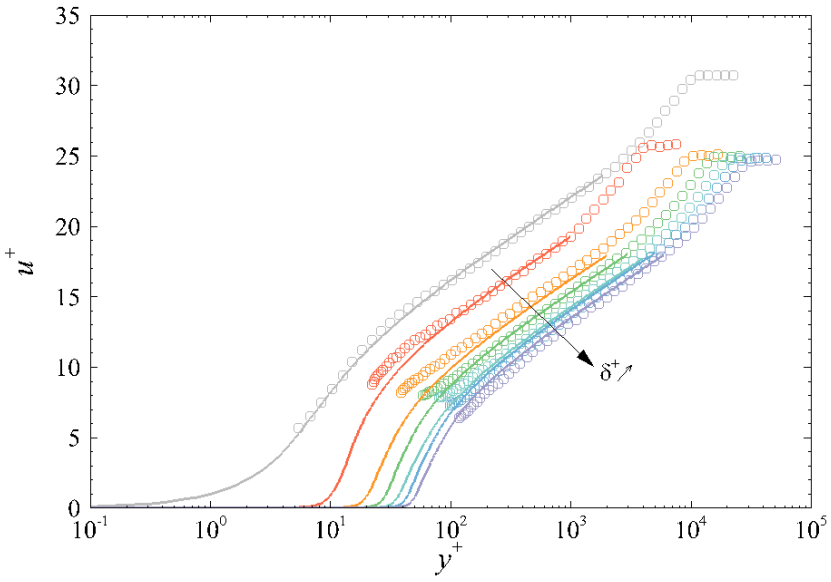

Figure 6. Comparison of streamwise mean velocity profile for all rough walls configurations. Symbols (○) show the experimental data and solid lines stand for the DANS computations. Gray color is used for the smooth configuration.

The importance of the mean elevation in predicting skin friction for flow over closely packed surface roughness. *Journal of Fluids Engineering* **128**, 579–586.

McClain, S.T., Hodge, B.K. & Bons, J.P. 2004 Predicting skin friction and heat transfer for turbulent flow over real gas turbine surface roughness using the discrete element method. *Journal of Turbomachinery* **126**, 259–267.

Menter, F.R. 1994 Two-equation eddy-viscosity turbulence models for engineering applications. *AIAA Journal* **32** (8), 1598–1605.

Nikuradse, J. 1937 Laws of flows in rough pipes. Technical Memorandum 1292. NACA, Washington.

Perry, A.E., Schofield, W.H. & Joubert, P.N. 1969 Rough wall turbulent boundary layers. *Journal of Fluid Mechanics* **37**, 383.

Robertson, J.A. 1961 Surface resistance as a function of the concentration and size of roughness elements. PhD thesis, State University of Iowa.

Schlichting, H. 1937 Experimental investigation of the problem of surface roughness. Technical Memorandum 823. NACA, Washington.

Squire, D.T., Hutchins, N., Morrill-Winter, C., Schultz, M.P., Klewicki, J.C. & Marusic, I. 2017 Applicability of taylor's hypothesis in rough- and smooth-wall boundary layers. *Journal of Fluid Mechanics* **812**, 398–417.

Stripf, M., Schulz, A., Bauer, H.J. & Wittig, S. 2009 Extended models for transitional rough wall boundary layers with heat transfer – Part I: Model formulations. *Journal of Turbomachinery* **131**, 031016–1 – 031016–10.

Stripf, M., Schulz, A. & Bauer, H.-J. 2008 Modeling of rough-wall boundary layer transition and heat transfer on turbine airfoils. *Journal of Turbomachinery* **130** (2).

Taylor, R.P., Coleman, H.W. & Hodge, B.K. 1985 Prediction of turbulent rough-wall skin friction using a discrete element approach. *Journal of Fluids Engineering* **107**, 251–257.

Whitaker, S. 1986 Flows in porous media I: A theoretical derivation of Darcy's law. *Transport in Porous Media* **1**, 3–25.

Whitaker, S. 1996 The forchheimer equation: A theoretical development. *Transport in Porous Media* **25**, 27–61.

Žukauskas, A. 1972 *Heat Transfer from Tubes in Crossflow*, *Advances in Heat Transfer*, vol. 8, pp. 93–160. J.P. Hartnett and T.F. Irvine.